Catalysis Today xxx (2015) xxx–xxx

Contents lists available at ScienceDirect

Catalysis Today

journal homepage: www.elsevier.com/locate/cattod

Impact of the synthesis route of supported copper catalysts on the performance in the methanol synthesis reaction

Roy van den Berg[a], Jovana Zečević[a], Jens Sehested[b], Stig Helveg[b], Petra E. de Jongh[a], Krijn P. de Jong[a,*]

[a] Inorganic Chemistry and Catalysis, Debye Institute for Nanomaterials Science, Utrecht University, Universiteitsweg 99, 3584 CG Utrecht, Netherlands
[b] Haldor Topsoe A/S, Haldor Topsøes Allé 1, DK-2800 Kgs. Lyngby, Denmark

ARTICLE INFO

Article history:
Received 18 June 2015
Received in revised form 14 August 2015
Accepted 24 August 2015
Available online xxx

Keywords:
Impregnation
Precipitation
Copper
Methanol synthesis
Sintering
Deactivation

ABSTRACT

Two Cu/SiO_2 methanol synthesis catalysts were synthesized, one via precipitation and one via impregnation. The copper particle size distribution and local copper weight loading were similar for both catalysts. Electron tomography revealed for the precipitated catalyst a plate-like silica structure with copper particles partially entrapped, whereas for the impregnated catalyst the copper particles were located in the pores between the primary particles of a silica gel. The precipitated catalyst displayed a lower initial copper weight normalized activity and a higher stability in the methanol synthesis reaction (40 bar, 260 °C). Copper particle growth during reaction, as determined by transmission electron microscopy, was more limited for the precipitated catalyst, in line with the higher catalyst stability, possibly due to the partial entrapment of the copper particles. In addition to copper particle growth, deactivation of both catalysts was ascribed to restructuring of the silica resulting in partial coverage of the copper surface.

1. Introduction

Supported metal catalysts are the workhorses of the chemical and petrochemical industry [1,2]. In general, catalysis takes place at the surface of the metal. Small particles and hence a high dispersion are therefore a prerequisite for a high activity. The role of the support is to facilitate the formation of small particles and to improve their thermal stability [3]. In some cases the support is also a chemical promoter, which increases the activity due to strong metal support interactions [4,5]. Despite the stabilizing effect of the support, metal particle growth is still one of the main causes for deactivation of cobalt and iron catalysts in the Fischer–Tropsch reaction [6,7], platinum and palladium in three-way catalysts [8,9], nickel catalysts in the methanation reaction [10], and copper catalysts in the water-gas shift and methanol synthesis reactions [11].

Particle growth can occur via particle diffusion and coalescence and via Ostwald ripening [12,13]. In the former mechanism, entire particles diffuse over the support surface until they meet each other and coalesce. In the latter, larger particles grow at the expense of smaller particles due to a net flux of metal-containing species from thermodynamically less stable smaller particles to more stable larger particles. Irrespective of the mechanism, particle growth is generally considered to depend on the reaction conditions [14], the metal-support interaction [15–17], the particle size (distribution) [18,19] and the interparticle spacing [20–22], and also on the geometry of the support [9,15,16,23,24]. It has for instance been shown that particle migration can be restricted by encagement or entrapment [23–27]. The geometry of the support can also affect the thermodynamic stability of a supported nanoparticle since the chemical potential of a supported nanoparticle depends on the contribution of the metal-support interfacial energy [3,28]. As a result, particles whose dimensions and volumes are commensurate with concavities in the support and hence have a large metal–support interface area tend to be more stable than particles on a flat support [28]. An increased metal–support interface area of the nanoparticle also leads to a decreased metal surface area accessible to the reactants and, hence, a lower activity. The optimal metal–support interface area is thus the one that provides a balance between nanoparticle activity and nanoparticle stability.

In industry two main routes are used to prepare supported metal catalysts, i.e. precipitation and impregnation [29]. In precipitation, a metal precursor is deposited on a preformed support (deposition–precipitation) or precipitated together with a support precursor (co-precipitation). Subsequent drying, calcination and reduction result in the formation of metallic particles and in the case of a co-precipitate also in the formation of the support

* Corresponding author.
E-mail address: K.P.deJong@uu.nl (K.P. de Jong).

http://dx.doi.org/10.1016/j.cattod.2015.08.052
0920-5861/

[30,31]. In impregnation, a support is contacted with a metal solution and metallic particles are formed upon drying, calcination and reduction [32]. The interface area between the metal particles and the support is dependent on the preparation route [33]. It might be larger in case of precipitation due to incomplete segregation [34–36]. During reaction the interface area might change due to a change in particle size, particle shape or support structure [28,37].

To study the effect of the synthesis method on the metal–support interaction and hence on metal nanoparticle activity and stability, we selected Cu/SiO_2 methanol synthesis catalysts as a model system. In such catalysts, the activity for CO/CO_2 hydrogenation scales with the copper surface area, and the loss of activity during reaction is often mainly due to copper particle growth [11,38,39]. Moreover, recent developments in the synthesis of well-defined copper on silica catalysts allow careful tuning of the size and distribution of the copper particles [40,41]. In this work Cu/SiO_2 catalysts with similar copper particle sizes and local copper weight loadings were synthesized via impregnation and via precipitation. Electron tomography was used to characterize the SiO_2 support structure and the location of the Cu particles within the support. The performance in the methanol synthesis reaction of both catalysts was investigated at 40 bar at 260 °C for a period of 10 days. The catalysts were retrieved after reaction to determine the extent of copper particle growth and change in support structure.

2. Material and methods

2.1. Synthesis of Cu/SiO_2 via precipitation

Precipitated Cu/SiO_2 was synthesized via a modified method of van der Grift et al. [42]. 20.1 g LUDOX-AS 30 (Sigma–Aldrich, 30 wt% SiO_2), 16.1 g $Cu(NO_3)_2{\cdot}3H_2O$ (Acros Organics, 99% for analysis) and 12.1 g Urea (Acros Organics, 99.5% for analysis) were added to 1.7 l of demineralized water in a 2 l reaction vessel. The pH was adjusted to 2–3 with a few drops of HNO_3 (Merck, 65% for analysis) to prevent premature hydrolysis of copper nitrate. The suspension was then heated to 90 °C over 1 h under stirring. At 90 °C the hydrolysis of urea led to an increase in pH resulting in precipitation of $Cu_2(NO_3)(OH)_3$. The well-stirred reaction vessel was kept at 90 °C for 7 days to allow recrystallization of precipitated copper and silica, which resulted in the formation of copper phyllosilicate [43,44]. The precipitate was obtained by hot filtration of the suspension and washed three times with demineralized water, filtered and dried overnight at 60 °C. The yield was 10 g. Part of the as-prepared copper phyllosilicate was used for catalytic reaction (with in situ reduction to obtain metallic Cu on SiO_2) as described below. Another part (2 g) intended for characterization was reduced at 250 °C (2 °C/min) in a flow of 100 ml/min of 20% H_2 in Ar for 2½ h. After the reduction treatment the resulting Cu/SiO_2 was passivated for 15 min by slowly exposing the sample to diluted air/N_2 at room temperature. The sample was stored in a glove box under argon atmosphere.

2.2. Synthesis of Cu/SiO_2 via impregnation

Copper was deposited on a commercial silica gel (Davicat 1454, Grace-Davison, pore volume $p/p_0 < 0.95 = 0.81\ cm^3/g$, pore diameter 9 nm) via incipient wetness impregnation with an aqueous solution of 2 M $Cu(NO_3)_2{\cdot}3H_2O$ (Acros Organics, 99% for analysis) and 0.1 M HNO_3 (Merck, 65% for analysis), followed by drying overnight under vacuum at room temperature and calcination in 375 ml/min (GHSV = 15,000 h^{-1}) of 2% NO/N_2 at 350 °C (2 °C/min) for 1 h. Part of the as-prepared sample was used for catalytic reaction (with in situ reduction to obtain metallic Cu on SiO_2) as described below and a portion (2 g) intended for characterization that underwent reduction in a flow of 100 ml/min of 20% H_2 in Ar at 250 °C (2 °C/min) for 2½ h. After the reduction treatment, the resulting Cu/SiO_2 was passivated for 15 min by slowly exposing the sample to diluted air/N_2 at room temperature. The sample was stored in a glove box under argon atmosphere.

2.3. Characterization

N_2-physisorption measurements were performed at −196 °C using a Micromeritics Tristar 3000 apparatus. The BET method was used to calculate the specific surface areas. The pore volumes were determined at $p/p_0 = 0.983$. Pore size distributions were determined from the adsorption branch by the BJH method [45]. X-ray diffraction (XRD) was performed with a Bruker-Nonius D8 Advance X-ray diffractiometer using Co-$K_{\alpha 12}$ ($\lambda = 1.79026$ Å) radiation. Diffractograms were collected at room temperature from 20° to 70° (2θ). The specimen holder was loaded in the glove box with the catalysts either after reduction and passivation or catalysis and passivation and was subsequently sealed. Copper crystallite sizes were estimated by applying the Debye–Scherrer equation to the (1 1 1) diffraction of Cu ($2\theta = 50.5°$, $k = 0.9$) [46]. H_2-TPD was performed on the catalysts before and after methanol synthesis [47,48]. Measurements were carried out in a fixed-bed flow setup and online gas analysis was performed by a quadrupole mass spectrometer (Balzers GAM 445). The copper phyllosilicate was reduced in situ at 250 °C (2 °C/min) in 100 ml/min of 1% H_2/He. At 250 °C the gas flow was changed to 100 ml/min of 100% H_2 for 2½ h. The calcined copper on silicagel and the samples after catalysis and passivation were reduced in situ at 220 °C (2 °C/min) in a flow 100 ml/min of 1% H_2/He for 7 h. Then the samples were flushed for ½ h in 100 ml/min of He to remove any adsorbed hydrogen and subsequently cooled down to 0 °C. At this temperature the reactor was pressurized to 1.6 MPa of H_2, before it was cooled down further to −33 °C. After ½ h, the catalyst was rapidly cooled to −196 °C and depressurized. The gas flow was changed to 100 ml/min of He to flush out the excessive hydrogen. After 1 h the temperature was increased up to 210 °C (6 °C/min) and the H_2 desorption profile was recorded. Copper surface areas ($SA_{Cu,\ H_2}$) were calculated from the amount of desorbed hydrogen assuming a H/Cu ratio of 0.5 and 1.47×10^{19} copper surface atoms per m^2. Temperature programmed reduction (TPR) was performed using an Autochem II ASAP 2910 from micromeritics. The H_2 concentration during the experiment was measured with a thermal conductivity detector. About 0.05 g of sample was put on top of a quartz wool bed in a glass reactor tube and subsequently heated to 500 °C (5 °C/min) under a (50 ml/min) flow of 5% H_2/Ar. The copper loading was estimated from the H_2 consumption by assuming the following reduction stoichiometry: $CuO + H_2 \rightarrow Cu + H_2O$. Transmission electron microscopy (TEM) images were acquired with a Tecnai 12 (FEI) microscope operated at 120 kV with a pixel size of 0.45 nm. Precipitated Cu/SiO_2 samples before and after catalytic tests were prepared by grinding followed by sonication in ethanol. A droplet of the ethanol suspension was deposited on a carbon coated copper TEM grid (Agar S162 200 Mesh Cu). The resolution and contrast were sufficient to detect particles larger than 2 nm (4 × 4 pixels). The impregnated Cu/SiO_2 was ground, embedded in a two component epoxy resin (Epofix, EMS) and cured at 60 °C overnight, and cut into thin sections (50–100 nm) using a Diatome Ultra 35° diamond knife mounted on an Ultracut E microtome (Reichert-Jung). Sections were deposited on a TEM grid. The resolution and contrast were sufficient to detect and measure particles larger than 3 nm (6 × 6 pixels). Copper surface areas ($SA_{Cu,\ TEM}$) were calculated from the particle size distributions obtained via TEM, and assuming spherical particles. Energy dispersive X-ray (EDX) spectroscopy was performed on a Technai 20FEG (FEI) electron microscope equipped with a field emission gun and an EDAX Super Ultra Thin Window EDX detector and

Please cite this article in press as: R. van den Berg, et al., Impact of the synthesis route of supported copper catalysts on the performance in the methanol synthesis reaction, Catal. Today (2015), http://dx.doi.org/10.1016/j.cattod.2015.08.052

processed with Tecnai Imaging and Analysis software. Samples were placed onto a carbon coated Ni TEM grid (Agar 162 200 Mesh Ni) and mounted on a low-background sample holder (Philips) with a 0.1 mm thick Be specimen support film and a Be ring to clamp the grid. The Cu/Si atomic ratio was determined for areas with a diameter of 100–500 nm from the integrated intensity of the Si–K and Cu–K signal. From that the weight loading of copper on silica was calculated.

2.4. Electron tomography

Electron tomography was performed on a Tecnai 20 (FEI) transmission electron microscope at 200 kV acceleration voltage in bright-field imaging mode. Quantifoil R2/1 Cu TEM grids with thin carbon film were used. The grids were wetted with a solution of 5 nm colloidal gold particles and subsequently dried. The gold particles acted as fiducial markers during the alignment. The catalyst samples were dispersed in ethanol and subsequently deposited on the grids. Tilt images were recorded from −70° to +70° with intervals of 2°. The resulting images were aligned to a common origin and rotation axis by tracking the 5 nm Au fiducial markers. 3D reconstruction of aligned tilt series was performed using a weighted back-projection algorithm in IMOD [49].

2.5. Catalytic testing

The performance of the catalysts in the methanol synthesis reaction was investigated in a fixed-bed stainless steel reactor with an inner diameter of 0.9 cm (Autoclave Engineers). The precipitated and impregnated Cu/SiO_2 prior to reduction were ground and sieved to obtain a sieve fraction of 0.42–0.63 mm. 0.55 g of the precipitated sample was diluted with SiC granules (sieve fraction of 0.25–0.42 mm) in a SiC: sample volume ratio of 1:4 and loaded into the reactor (catalyst bed height of 7 cm). 0.81 g of the impregnated sample was loaded into the reactor (catalyst bed height of 5 cm) without dilution. Subsequently, both samples were reduced in situ at 250 °C (2 °C/min) for 2.5 h with a flow of 110 ml/min 20% H_2/Ar. After that, the temperature was lowered to 100 °C to prevent premature production of methanol when switching to syngas. The reactor was flushed with syngas (10% Ar, 7% CO_2, 23% CO, 60% H_2, Linde), which was purified with a metal carbonyl trap [50] (4.0 g of 0.5–1.5 mm H-USY zeolite, CVB-780 from Zeolyst Int. and 5 g activated carbon, Norit R3B). The argon in the syngas feed acted as an internal standard for the gas chromatograph (GC). After 30 min of flushing the pressure was increased to 40 bar. From this time on the exit gas composition was analyzed every 110 min with a GC (Varian 450). The lines from the reactor to the GC were heated to 150 °C to avoid any methanol or water condensation. The first GC channel consisted of a HAYESEP Q (0.5 M × 1.8 in.) column followed by a MOLSIEVE 13x (15 × 1/8 in.) column that led to a thermal conductivity detector (TCD). The second GC channel consisted of a CP-SIL 8CB FS capillary column that led to a flame ionization detector (FID). Three chromatograms were recorded of the syngas feed. The temperature was then increased to 260 °C (2 °C/min) to initiate methanol production. The amount of catalyst and the syngas flow (10–30 ml/min) were chosen such that CO conversion levels near 15% were obtained. The activity of the catalyst was determined by the conversion of CO and CO_2 during reaction. The deviation in between different tests in the initial activity is ±35% and in the deactivation ±3%. Turnover frequencies (TOF) were calculated with the assumption that one copper surface atom is an active site. The initial and final (at the end of the catalytic testing) amount of active sites was based upon H_2-TPD before and after reaction, respectively. The selectivity was determined from the FID chromatograms and was in all cases more than 98.5% towards methanol, with trace amounts of dimethyl ether, methane, ethanol, ethane and propane. The stability of the methanol productivity over time was based upon the methanol signal from the TCD detector. Second order deactivation constants were calculated according to the formula: $1/a = 1 + k_{d,2} * t$ [3], in which a is the activity, $k_{d,2}$ is the second order deactivation constant and t is the time. After catalysis the samples were passivated for 15 min by slowly exposing the sample to air diluted with Ar at room temperature. The sample was stored in a glove box under argon atmosphere.

3. Results and discussion

3.1. Characterization of Cu/SiO_2

Cu/SiO_2 was prepared via either precipitation or incipient wetness impregnation (Fig. 1A–D). For the precipitated catalyst, XRD of the reduced and passivated sample showed that reduction at 250 °C in a flow of 20% H_2 in Ar for 2½ h resulted in the reduction of precipitated copper phyllosilicate to metallic copper with an average crystallite size of 5.2 nm and silica (Fig. 1A), in line with literature [44,51]. TEM showed the presence of 8 nm sized copper particles homogeneously distributed over the silica support after reduction and passivation (Fig. 1B). The copper loading as determined with TPR was 40.1 wt%, which corresponds well to the theoretical amount of 41 wt% based on quantitative deposition. The local copper loading measured with TEM-EDX was 38 ± 1 wt% (five different locations), in agreement with the bulk copper loading.

Incipient wetness impregnation with a 2 M aqueous copper nitrate solution of commercially available silica gel with an average pore diameter of 9 nm, followed by drying, calcination in NO/N_2 flow, reduction and passivation, resulted in 8 nm sized copper particles, in high-density domains of a couple of hundred nanometers to even micrometers, as determined by TEM (Fig. 1D). The bulk copper loading in this catalyst as determined with TPR was 8.6 wt%, which corresponds to the nominal loading of 9.0 wt%. EDX revealed a weight loading of 37 ± 6% (9 locations) copper on silica within the high-density domains of particles, while other parts of the silica support were almost empty (<1 wt% Cu, 6 locations). These domains are a consequence of the drying and calcination process [40,22]. In a flow of 2% NO/N_2, non-mobile $Cu_2NO_3(OH)_3$ is nucleated, which might grow larger from mobile $Cu(NO_3)_2{\cdot}3H_2O$. As a result, $Cu_2NO_3(OH)_3$ completely filled up the pores in some regions while the pores in other regions were left empty. The maximum amount of copper within a region, assuming a density of $Cu_2NO_3(OH)_3$ of 1.675 g/cm^3 [41,52] and a silica pore volume of 0.81 ml/g, was calculated to be 41 wt%. This is in close accordance to the observed copper loading within the high-density domains. Upon further decomposition in NO/N_2 flow and reduction using H_2, metallic copper particles with an average copper crystallite size of 8.7 nm were formed, as determined from XRD after reduction and passivation (Fig. 1 C). The final size of the copper particles (~8 nm) was close to the size of the pores of the silica support (~9 nm) as found before [41,53]. Both Cu/SiO_2 prepared via impregnation and via precipitation thus consisted on a local scale of a similar loading of similarly sized copper particles.

N_2-physisorption was used to assess the porosity of the impregnated and precipitated Cu/SiO_2 after reduction and passivation (Fig. 2A–D and Table 1). The physisorption isotherms were markedly different for both samples. The impregnated Cu/SiO_2 had a type H2 hysteresis loop which is generally obtained for porous materials consisting of agglomerates of approximately uniform spheres like silica gel [54]. The pore size distribution was relatively narrow with a maximum near 9 nm (Fig. 2B). The precipitated Cu/SiO_2 displayed a type H4 hysteresis loop which is associated with slit-like pores and typical for aggregates of plates [42,55]. As a

Please cite this article in press as: R. van den Berg, et al., Impact of the synthesis route of supported copper catalysts on the performance in the methanol synthesis reaction, Catal. Today (2015), http://dx.doi.org/10.1016/j.cattod.2015.08.052

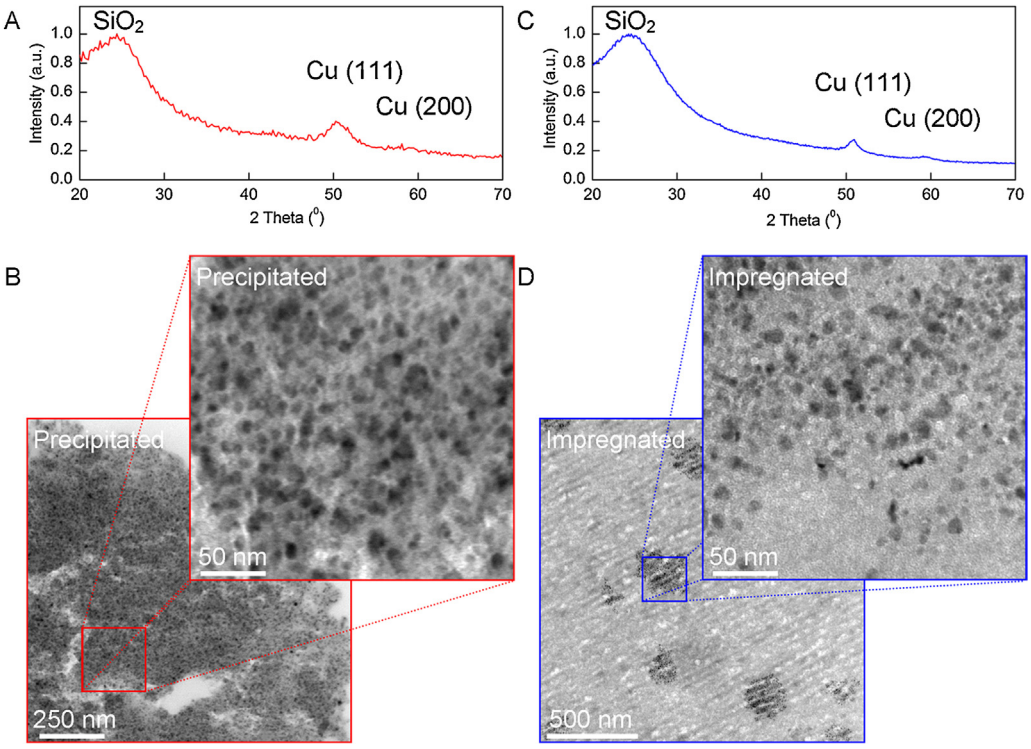

Fig. 1. X-ray diffractograms of Cu/SiO_2 after reduction and passivation prepared via either precipitation (A) or incipient wetness impregnation (C). TEM images at lower (bottom left) and higher (top right) magnifications of Cu/SiO_2 after reduction and passivation prepared via either precipitation (B) or incipient wetness impregnation (D).

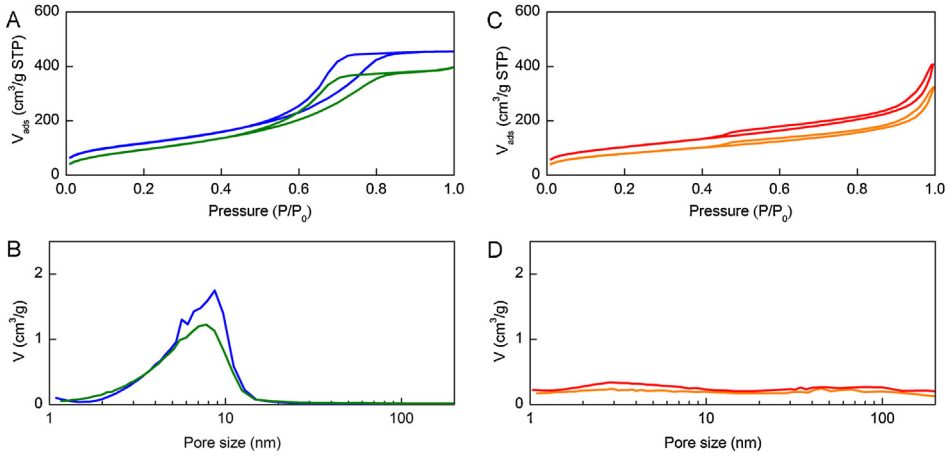

Fig. 2. N_2-physisorption isotherms (A) and corresponding pore size distributions (B) after reduction and passivation (blue) and after catalysis and passivation (green) of Cu/SiO_2 prepared via impregnation. N_2-physisorption isotherms (C) and corresponding pore size distributions (D) after reduction and passivation (red) and after catalysis and passivation (orange) of Cu/SiO_2 prepared via precipitation.

Table 1
Data derived from N_2-physisorption for fresh and spent catalysts.

	After reduction and passivation		After catalysis and passivation	
	BET surface area (m^2/g_{cat})	Pore volume (cm^3/g_{cat})	BET surface area (m^2/g_{cat})	Pore volume (m^2/g_{cat})
Precipitated Cu/SiO_2	375	0.59	290	0.46
Impregnated Cu/SiO_2	430	0.70	365	0.61

result, the pore size distribution was very broad with macropores (>50 nm) next to mesopores (2–50 nm; Fig. 2D).

Electron tomography was used to visualize the support structure and the 3D location of the copper particles within the silica support [22,56]. Fig. 3A and B shows tomogram thin sections of the precipitated Cu/SiO_2 after reduction and passivation. In Fig. 3A the silica support shows a plate-like structure with different pore sizes. This is in line with the broad pore size distribution found from N_2-physisorption. Careful analysis going through the material section by section at higher magnifications indicated that some copper

Please cite this article in press as: R. van den Berg, et al., Impact of the synthesis route of supported copper catalysts on the performance in the methanol synthesis reaction, Catal. Today (2015), http://dx.doi.org/10.1016/j.cattod.2015.08.052

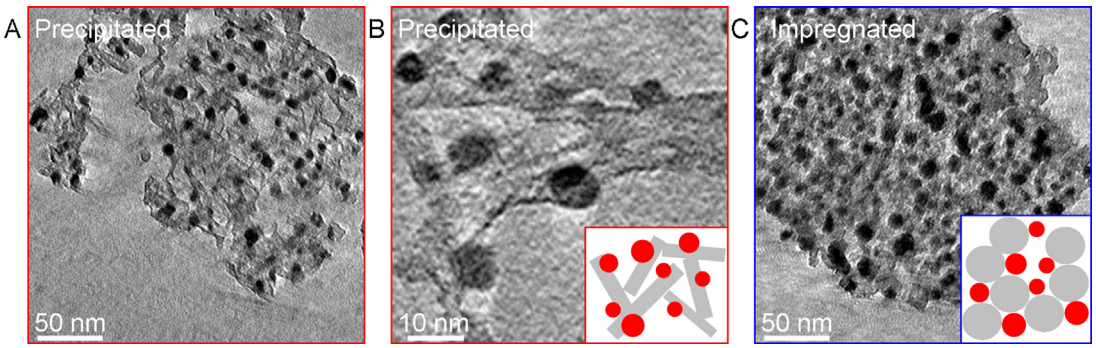

Fig. 3. Electron tomogram sections of precipitated ((A) and (B)) and impregnated (C) Cu/SiO_2. The thickness of numerical section (A) and (C) is 3.6 nm, the thickness of numerical section (B) is 0.56 nm. Schematic representations of the copper (red) and silica (grey) in both catalysts are depicted in the bottom right of (B) and (C).

particles (darker image features) were at least partially embedded within the silica, as shown in Fig. 3B and illustrated in the scheme at the bottom right of Fig. 3B (see Supplementary Information for a movie of the reconstructed volume). Fig. 3C shows a tomogram section of the impregnated Cu/SiO_2 after reduction and passivation. In this case the copper particles were located in between the silica primary particles as illustrated in the scheme at the bottom right of the figure. The porosity in this sample was harder to resolve compared to the precipitated sample, due to the narrower pores located within more dense Cu/SiO_2 aggregates of several hundreds of nanometers. Despite the similar local weight loadings, the interparticle distances seem to be smaller for the impregnated catalyst. The higher volumetric copper loading might be due to the lower porosity in the impregnated silica gel (Fig. 2).

H_2-TPD was used to determine the accessible copper surface area of the two catalysts (Table 2). For the precipitated catalyst the specific copper surface area measured with H_2-TPD was about 33% lower than the one based on the TEM particle size distributions, probably due to partial entrapment of the copper particles as suggested by electron tomography. For the impregnated copper on silica the copper surface area inaccessible for H_2 adsorption was insignificant, indicating a less extensive metal–support interface area for this catalyst.

3.2. Catalytic performance

The performance of impregnated and precipitated Cu/SiO_2 was investigated in the methanol synthesis reaction at 40 bar, 260 °C at 15% CO conversion. The selectivity towards methanol was above 98.5%. The methanol synthesis productivity was calculated from the conversion of $CO + CO_2$ (Table 3). The TOFs of the catalysts were between 2.0 and 4.0×10^{-3} s^{-1}, in close accordance with previously reported values for copper on silica [39,41,57,58]. The copper weight-based methanol productivity as well as the TOF based on the copper surface area measured with H_2-TPD was lower for the precipitated catalyst (Table 3). Robbins et al. have reported that the activity for Cu/SiO_2 catalysts in the methanol synthesis reaction from a mixture of CO and CO_2, scales linearly with the metallic copper surface area [39,59]. The lower TOF for the precipitated catalyst indicates that for this sample even less copper surface area had been available for methanol synthesis than was indicated by H_2-TPD.

The loss in activity over time was less for the precipitated catalyst than for the impregnated catalyst resulting in a lower second-order deactivation constant (Fig. 4 and Table 3). For both catalysts the deactivation corresponded to the loss of accessible copper surface area upon reaction as determined by H_2-TPD (Table 2). To determine the loss of copper surface area due to copper particle growth, the particle size distributions after catalysis and passivation were determined with TEM (Fig. 5). For the precipitated catalyst the particle size distribution had increased from 8.0 ± 2.2 nm to 8.6 ± 2.6 nm and for the impregnated catalyst from 8.3 ± 2.6 nm to 9.2 ± 2.7 nm. Analysis of the variance in the size distribution showed that the increase in particle size is statistically significant for both samples ($p_{(\text{same mean size})} \ll 0.001$). The copper crystallite size as determined with XRD had increased from 5.2 to 5.8 nm for the precipitated catalyst and from 8.7 to 9.2 nm for the impregnated catalyst (Fig. 6). For both catalysts, the increase in crystallite size had been similar to the increase in particle size. The precipitated catalyst had thus been more resistant against particle growth in line with the higher catalyst stability in the methanol synthesis reaction. The higher nanoparticle stability for the precipitated catalyst might have been due to a stronger metal–support interaction [3,28]. For the short interparticle distances (<5 nm), particle migration and coalescence has been identified to significantly contribute to particle growth [13,22]. Electron tomography indicated for the precipitated catalyst that the particles were partially entrapped in the silica support, possibly limiting their mobility due to the increased metal–support interface area [3,28].

Particle growth only explained part of the loss of copper surface area, especially in the case of the impregnated catalyst, indicating that secondary effects like copper surface blockage by silica also play a role. N_2-physisorption measurements after catalysis and passivation showed a significant decrease of pore volume and BET surface area for both catalysts (Fig. 2 and Table 1). Silica restructuring during reaction had taken place and probably led to reduced gas accessibility of the copper surface by e.g. partial coverage. Since for the impregnated catalyst the size of the copper particles was close to the size of the pores, the metal–support interface area might furthermore have been increased during reaction due to growth of the copper particles or due to shrinkage of the pores [28]. Previously it has been reported that the support in $CuZn/SiO_2$

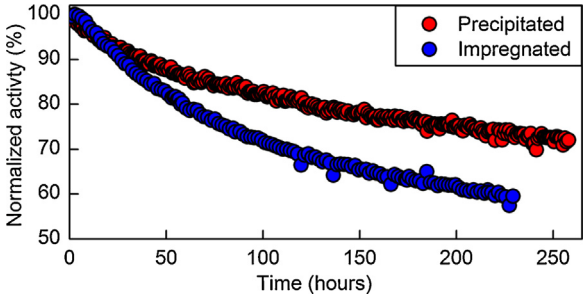

Fig. 4. Normalized activity over time for Cu/SiO_2 prepared via precipitation (red) and via impregnation (blue).

Please cite this article in press as: R. van den Berg, et al., Impact of the synthesis route of supported copper catalysts on the performance in the methanol synthesis reaction, Catal. Today (2015), http://dx.doi.org/10.1016/j.cattod.2015.08.052

Table 2
Specific copper surface areas before and after reaction based on H_2-TPD and TEM.

	Before reaction		After reaction	
	$SA_{cu,TEM}$ (m^2_{cu}/g_{cu})	SA_{cu,H_2} (m^2_{cu}/g_{cu})	$SA_{cu,TEM}$ (m^2_{cu}/g_{cu})	SA_{cu,H_2} (m^2_{cu}/g_{cu})
Precipitated Cu/SiO_2	73	48	65	39
Impregnated Cu/SiO_2	68	67	62	38

Table 3
Catalytic performance of Cu/SiO_2 in the methanol synthesis at 260 °C and 40 bar; TOF values based on H_2-TPD.

	Initial MeOH productivity (mol MeOH $kg_{cu^{-1}}$ h^{-1})	Initial TOF (s^{-1})	Final TOF (s^{-1})	Deactivation constant (h^{-1})
Precipitated Cu/SiO_2	8.8 ± 3.1	$2.1 \pm 0.7 \times 10^{-3}$	$1.9 \pm 0.7 \times 10^{-3}$	0.0023
Impregnated Cu/SiO_2	20.5 ± 7.2	$3.5 \pm 1.2 \times 10^{-3}$	$3.6 \pm 1.3 \times 10^{-3}$	0.0033

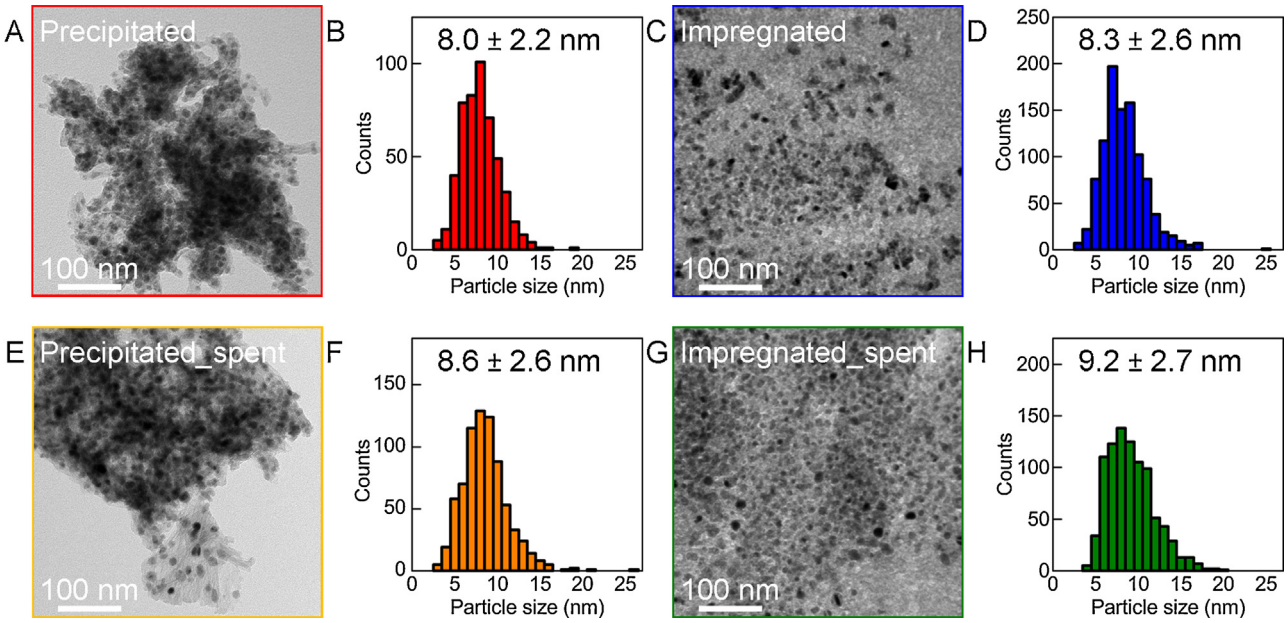

Fig. 5. TEM images and corresponding particle size distributions of Cu/SiO_2 prepared via precipitation before (A, B) and after reaction (E, F). TEM images and corresponding particle size distributions of Cu/SiO_2 prepared via impregnation before (C, D) and after reaction (G, H).

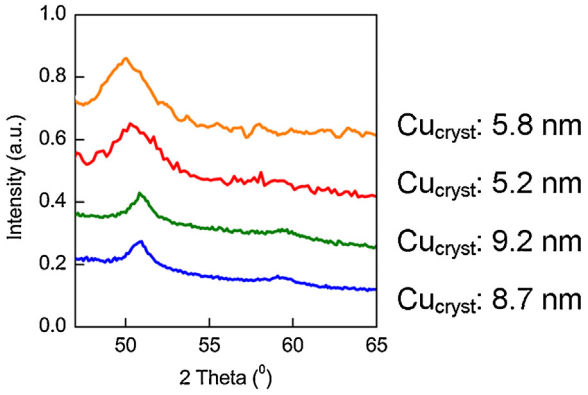

Fig. 6. X-ray diffractograms of Cu/SiO_2 prepared via impregnation before (blue) and after reaction (green) and of Cu/SiO_2 prepared via precipitation before (red) and after reaction (orange). Corresponding crystallite sizes (Cu_{cryst}) are displayed next to the respective diffractogram.

catalysts was stable during the methanol synthesis at similar conditions [23]. During synthesis of these catalysts, co-impregnation of copper and zinc led to the incorporation of zinc in the silica support, resulting in a zinc-silicate, which is more stable than ZnO and SiO_2 separately [60].

4. Conclusions

Cu/SiO_2 catalysts with similar copper particle size and local copper loading were synthesized via either precipitation or incipient wetness impregnation. Electron tomography revealed for the precipitated catalyst a plate-like silica structure with copper particles partially entrapped, whereas for the impregnated catalyst the copper particles were located in the pores between the primary particles of the silica gel. For the precipitated catalyst, the initial copper-weight normalized activity in the methanol synthesis reaction was lower, but catalyst stability higher partly due to more limited copper particle growth. Additionally, silica restructuring during reaction had occurred and resulted in catalyst deactivation attributed to partial coverage of the copper surface. Partial entrapment of the copper particles, achieved via precipitation and subsequent reduction, can hence lead to lower catalyst activity but at the same time to higher catalyst stability.

Acknowledgements

The project was supported financially by Haldor Topsoe A/S, Denmark. The authors are grateful to Grace, in particular to Robert Goedvree, for providing the silica gel support. Sebastian Kuld is acknowledged for H_2-TPD measurements. Hans Meeldijk is acknowledged for microtomy and TEM-EDX analysis.

Please cite this article in press as: R. van den Berg, et al., Impact of the synthesis route of supported copper catalysts on the performance in the methanol synthesis reaction, Catal. Today (2015), http://dx.doi.org/10.1016/j.cattod.2015.08.052

Appendix A. Supplementary data

Supplementary data associated with this article can be found, in the online version, at http://dx.doi.org/10.1016/j.cattod.2015.08.052.

References

[1] A.T. Bell, Science 299 (2003) 1688–1691.
[2] H.M. Torres Galvis, J.H. Bitter, C.B. Khare, M. Ruitenbeek, A.I. Dugulan, K.P. de Jong, Science 335 (2012) 835–838.
[3] C.H. Bartholomew, Appl. Catal. A 107 (1993) 1–57.
[4] T. Lunkenbein, J. Schumann, M. Behrens, R. Schlogl, M.G. Willinger, Angew. Chem. Int. Ed. 127 (2015) 1–6.
[5] S.J. Tauster, S.C. Fung, R.T.K. Baker, J.A. Horsley, Science 211 (1981) 1121–1125.
[6] J. van de Loosdrecht, F.G. Botes, I.M. Ciobica, A. Ferreira, P. Gibson, D.J. Moodley, A.M. Saib, J.L. Visagie, C.J. Weststrate, J.W. Niemantsverdriet, Fischer–Tropsch synthesis: catalysts and chemistry, in: J. Reedijk, K. Poeppelmeier (Eds.), Comprehensive Inorganic Chemistry II, Elsevier, Oxford, 2013, pp. 525–557.
[7] P. Munnik, P.E. de Jongh, K.P. de Jong, J. Am. Chem. Soc. 136 (2014) 7333–7340.
[8] J.A. Moulijn, A.E.V. Diepen, F. Kapteijn, Science 212 (2001) 3–16.
[9] S.B. Simonsen, I. Chorkendorff, S. Dahl, M. Skoglundh, J. Sehested, S. Helveg, J. Am. Chem. Soc. 132 (2010) 7968–7975.
[10] P. Munnik, M.E.Z. Velthoen, P.E. de Jongh, K.P. de Jong, C.J. Gommes, Angew. Chem. Int. Ed. 126 (2014) 9647–9651.
[11] M.V. Twigg, M.S. Spencer, Appl. Catal. A 212 (2001) 161–174.
[12] B. Pulvermacher, J. Catal. 245 (1973) 224–245.
[13] I.M. Lifshitz, V.V. Slyozov, J. Phys. Chem. Solids 19 (1961) 35–50.
[14] D.B. Rasmussen, T.V.W. Janssens, B. Temel, T. Bligaard, B. Hinnemann, S. Helveg, J. Sehested, J. Catal. 293 (2012) 205–214.
[15] A. Cao, R. Lu, G. Veser, Phys. Chem. Chem. Phys. 12 (2010) 13499–13510.
[16] R. Ouyang, J.-X. Liu, W.-X. Li, J. Am. Chem. Soc. 135 (2013) 1760–1771.
[17] W.T. Wallace, B.K. Min, D.W. Goodman, J. Mol. Catal. A: Chem. 228 (2005) 3–10.
[18] C.T. Campbell, S.C. Parker, D.E. Starr, Science 298 (2002) 811–814.
[19] A.K. Datye, Q. Xu, K.C. Kharas, J.M. McCarty, Catal. Today 111 (2006) 59–67.
[20] K. Morgenstern, G. Rosenfeld, G. Comsa, Surf. Sci. 441 (1999) 289–300.
[21] S.B. Simonsen, I. Chorkendorff, S. Dahl, M. Skoglundh, J. Sehested, S. Helveg, J. Catal. 281 (2011) 147–155.
[22] G. Prieto, J. Zečević, H. Friedrich, K.P. de Jong, P.E. de Jongh, Nat. Mater. 12 (2013) 34–39.
[23] G. Prieto, M. Shakeri, K.P. de Jong, P.E. de Jongh, ACS Nano 8 (2014) 2522–2531.
[24] P.M. Arnal, M. Comotti, F. Schuth, Angew. Chem. Int. Ed. 45 (2006) 8224–8227.
[25] S.H. Joo, J.Y. Park, C.K. Tsung, Y. Yamada, P. Yang, G.A. Somorjai, Nat. Mater. 8 (2009) 126–131.
[26] J. Lu, B. Fu, M.C. Kung, G. Xiao, J.W. Elam, H.H. Kung, P.C. Stair, Science 335 (2012) 1205–1208.
[27] A.B. Laursen, K.T. Hojholt, L.F. Lundegaard, S.B. Simonsen, S. Helveg, F. Schuth, M. Paul, J.D. Grunwaldt, S. Kegnaes, C.H. Christensen, K. Egeblad, Angew. Chem. Int. Ed. 49 (2010) 3504–3507.
[28] P. Wynblatt, N.A. Gjostein, Prog. Solid State Chem. 9 (1976) 21–58.
[29] K.P. de Jong (Ed.), Synthesis of Solid Catalysts, Wiley-VCH, Weinheim, 2009.
[30] C. Baltes, S. Vukojevic, F. Schuth, J. Catal. 258 (2008) 334–344.
[31] S.-I. Fujita, S. Moribe, Y. Kanamori, M. Kakudate, N. Takezawa, Appl. Catal. A 207 (2001) 121–128.
[32] A.V. Neimark, L.I. Kheifez, V.B. Fenelonov, Ind. Eng. Chem. Prod. Res. 20 (1981) 439–450.
[33] T. Montini, A.M. Condò, N. Hickey, F.C. Lovey, L. De Rogatis, P. Fornasiero, M. Graziani, Appl. Catal. B 73 (2007) 84–97.
[34] M. Behrens, A. Furche, I. Kasatkin, A. Trunschke, W. Busser, M. Muhler, B. Kniep, R. Fischer, R. Schlögl, ChemCatChem 2 (2010) 816–818.
[35] M. Behrens, I. Kasatkin, S. Kühl, G. Weinberg, Chem. Mater. 22 (2010) 386–397.
[36] S. Kuhl, A. Tarasov, S. Zander, I. Kasatkin, M. Behrens, Chem. Eur. J. 20 (2014) 3782–3792.
[37] P.L. Hansen, J.B. Wagner, S. Helveg, J.R. Rostrup-Nielsen, B.S. Clausen, H. Topsoe, Science 295 (2002) 2053–2055.
[38] J.B. Hansen, P.E. Hojlund Nielsen, Methanol synthesis, in: G. Ertl, H. Knozinger, F. Schuth, J. Weltkamp (Eds.), Handbook of Heterogeneous Catalysis, Wiley-VCH, 2008, pp. 2920–2949.
[39] J.L. Robbins, E. Iglesia, C.P. Kelkar, B. DeRites, Catal. Lett. 10 (1991) 1–10.
[40] P. Munnik, M. Wolters, A. Gabrielsson, S.D. Pollington, G. Headdock, J.H. Bitter, P.E. de Jongh, K.P. de Jong, J. Phys. Chem. C 115 (2011) 14698–14706.
[41] G. Prieto, J.D. Meeldijk, K.P. de Jong, P.E. de Jongh, J. Catal. 303 (2013) 31–40.
[42] C.J.G. van der Grift, P.A. Elberse, A. Mulder, J.W. Geus, Appl. Catal. 59 (1990) 275–289.
[43] T. Toupance, M. Kermarec, J.-F. Lambert, C. Louis, J. Phys. Chem. B 106 (2002) 2277–2286.
[44] L. Chen, P. Guo, M. Qiao, S. Yan, H. Li, W. Shen, H. Xu, K. Fan, J. Catal. 257 (2008) 172–180.
[45] E.P. Barret, L.G. Joyner, P.P. Halenda, J. Am. Chem. Soc. 73 (1951) 373–380.
[46] A.L. Patterson, Phys. Rev. 56 (1939) 978–982.
[47] M. Muhler, L.P. Nielsen, E. Tornqvist, B.S. Clausen, H. Topsoe, Catal. Lett. 14 (1992) 241–249.
[48] T. Genger, O. Hinrichsen, M. Muhler, Catal. Lett. 59 (1999) 137–141.
[49] J.R. Kremer, D.N. Mastronarde, J.R. McIntosh, J. Struct. Biol. 116 (1996) 71–76.
[50] C.J. Smit, R. Eijkhoudt, J.W. Geus, A.J. Van Dillen, Am. Chem. Soc., Div. Fuel Chem. 44 (1999) 119–123.
[51] J. Gong, H. Yue, Y. Zhao, S. Zhao, L. Zhao, J. Lv, S. Wang, X. Ma, J. Am. Chem. Soc. 134 (2012) 13922–13925.
[52] N. Guillou, M. Louer, D. Louer, J. Solid State Chem. 109 (1994) 307–314.
[53] A.Y. Khodakov, A. Griboval-Constant, R. Bechara, F. Villain, J. Phys. Chem. B 105 (2001) 9805–9811.
[54] K.S.W. Sing, Pure Appl. Chem. 54 (1982) 2201–2218.
[55] Z. Huang, F. Cui, J. Xue, J. Zuo, J. Chen, C. Xia, J. Phys. Chem. C 114 (2010) 16104–16113.
[56] P.A. Midgley, R.E. Dunin-Borkowski, Nat. Mater. 8 (2009) 271–280.
[57] van den Berg et al. Please note that these values are slightly lower than those reported in reference [41], as we found the calculation in [41] not to be fully correct. The correct calculation procedure can be found in reference [58].
[58] R. van den Berg, T.E. Parmentier, C.F. Elkjaer, C.J. Gommes, J. Sehested, S. Helveg, P.E. de Jongh, K.P. de Jong, ACS Catal. 5 (2015) 4439–4448.
[59] K.C. Waugh, Catal. Lett. 142 (2012) 1153–1166.
[60] I. Barin, Thermochemical Data of Pure Substances, 3rd ed., VCH Wiley, Weinheim, 1995.

Please cite this article in press as: R. van den Berg, et al., Impact of the synthesis route of supported copper catalysts on the performance in the methanol synthesis reaction, Catal. Today (2015), http://dx.doi.org/10.1016/j.cattod.2015.08.052